ACS OMEGA

http://pubs.acs.org/journal/acsodf

Article

In Situ Synthesis of Metal-Containing ZSM-5 and Its Catalytic Performance in Aromatization of Methanol

Yanjun Zhang, Yao Liu, and Jianwei Li*

Cite This: *ACS Omega* 2022, 7, 24241−24248

Read Online

ACCESS | Metrics & More | Article Recommendations

ABSTRACT: Metal-containing ZSM-5 zeolites, denoted as M/ZSM-5 (M = Ga, Zn, and La), were prepared by an in situ synthetic method. The structural, textural, and surface acid properties of M/ZSM-5 were characterized by XRD, N_2 adsorption−desorption, NH_3-TPD, and FT-IR. The catalyst pore size and the distribution of strong acid and weak acid were affected by the introduction of metal. Considering the methanol-to-aromatics model reaction, the catalytic performance of these samples was investigated in a fixed bed reactor under the conditions of 450 °C and a liquid weight hourly space velocity (WHSV) of 5 h^{-1}. The results indicated that the Zn/ZSM-5 molecular sieve was most beneficial to aromatization; the relationship between the change of B/L caused by Zn content and aromatics selectivity was further studied. When the B/L value decreased, the selectivity of aromatics showed an initial increase and then a decrease. The B/L value was optimal, and the aromatics yield was the highest when the Zn loading was 0.35%.

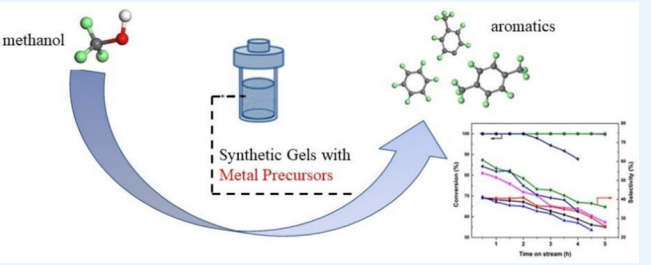

1. INTRODUCTION

Benzene, toluene, and xylene (BTX) are widely used as important industrial intermediates with increasing demand every year.[1−3] The main methods for producing BTX are catalytic reforming and steam cracking of naphtha.[4,5] However, as petroleum resources are limited with erratic prices, it is of paramount importance for governments and researchers to find a nonoil route to produce these aromatics. In recent years, methanol has been able to be obtained from various resources such as coal and biomass, resulting in an overcapacity of methanol.[2,6,7] Coincidentally, methanol aromatization can solve the problem of the BTX shortage and excess methanol.

Methanol aromatization is a complex reaction system involving numerous side reactions. The distribution and content of methanol aromatization products are related to the reaction conditions, molecular sieve structure, and acidity.[8−10] In the methanol aromatization reaction, the ZSM-5 molecular sieve has become the most promising catalyst due to its superior shape-selective catalytic performance, hydrothermal stability, and adjustable acidity.[11−14] Many researchers have modified the ZSM-5 molecular sieve to improve the yield of aromatic hydrocarbons using methods such as hydrothermal modification, acid−base modification, metal modification, etc.[15−18] Among them, metal modification has shown the most improvement in catalytic performance to achieve a higher aromatics yield.

The methods of synthesizing a metal bifunctional ZSM-5 molecular sieve include dipping, ion exchange, and isomorphous substitution. Pan et al.[19] successfully introduced Zn into the ZSM-5 molecular sieve by impregnation and isomorphous substitution methods, separately. The experimental results showed that H [Zn, Al] ZSM-5/SiO_2 obtained by isomorphous substitution possessed more strong and medium acid sites, beneficial to cyclization and aromatization in the methanol-to-aromatics (MTA) reaction. The presence of more intercrystalline voids improved the carbon deposition resistance of the catalyst. Niu et al.[20] synthesized Zn-containing HZSM-5 zeolites by ion exchange, impregnation, mechanical mixing, and direct synthesis, separately, to influence the nature of the Zn species and acid distribution. Molecular sieves synthesized by direct synthesis with small particle size and high mesoporous volume with a suitable ratio of B acid to L acid exhibited the highest selectivity for aromatics and the longest catalytic lifetime. The ZSM-5 molecular sieve with low Si/Al is suitable for the MTA reaction, but when the content of framework aluminum is low, the degree of metal cation exchange by the ion exchange method is limited,[21] and the metal species formed by the impregnation method exist as large metal oxide clusters that block the pores or cover the external surface.[22] The metal distribution of in situ synthesis is

Received: March 10, 2022
Accepted: June 24, 2022
Published: July 10, 2022

https://doi.org/10.1021/acsomega.2c01442
ACS Omega 2022, 7, 24241−24248

more dispersed, and the synthesis is more convenient, omitting the postprocessing step.

Su et al.[23] obtained nanosized H-ZSM-5 zeolites isomorphously substituted by Ga and tested their catalytic performances in the 1-hexene and FCC gasoline aromatization. The Ga isomorphous substitution can facilitate the formation of both B and L acid sites, leading to higher aromatic yield. Zhang et al.[24] prepared an Fe-modified ZSM-5 via a direct method used for the conversion of biomass to light olefins, with the results showing that the Fe-modified ZSM-5 catalyst increased the olefins yield significantly. These above experiments prove that transition metals can be synthesized in situ into molecular sieves to provide excellent catalytic properties.

In this work, we introduced three metals (Ga, La, and Zn) by in situ synthesis, a process more convenient than ion exchange and impregnation, to investigate the effects of these three kinds of metals and Zn content on the reaction of methanol to aromatics. The relationship between the B/L of molecular sieves with different Zn contents and their aromatic selectivity was studied. The results provide a reference for a simple preparation method of metal-containing molecular sieves and suitable metal loading used in the methanol-to-aromatics reaction.

2. EXPERIMENTAL SECTION

2.1. Synthesis of the M/ZSM-5 Molecular Sieve. ZSM-5 zeolite was synthesized with the molar composition of SiO_2:0.026Al_2O_3:0.2Na_2O:0.15NaCl:0.2DEA:25H_2O from a mixture of sodium hydroxide (NaOH, AR), sodium chloride (NaCl, AR), silica sol (40 wt % SiO_2, 0.4 wt % Na_2O), aluminum sulfate octadecahydrate ($Al_2(SO_4)_3 \cdot 18H_2O$, AR), and diethylamine (DEA, AR). The prereaction and the crystallization were conducted at 100 °C for 24 h and 170 °C for 72 h in a rotating Teflon-lined stainless steel autoclave (200 rpm), respectively. The solid products were recovered by centrifugation and washed with deionized water repeatedly until the mother liquid showed a pH value of 7−8, followed by drying at 100 °C overnight and calcination at 550 °C for 6 h in air. The hydrogen type ZSM-5 zeolite was obtained through ion-exchanging with an aqueous NH_4NO_3 solution at 80 °C for 12 h and subsequent calcination at 550 °C for 4 h. The HZSM-5 zeolite is marked S-0.

Selected amounts of $GaCl_3 \cdot 6H_2O$, $La(NO_3)_3 \cdot 6H_2O$, or $ZnCl_2$ are added to the above sol (before transfer to autoclave) to obtain S-1 (0.15% Ga), S-2 (0.15% La), S-3 (0.15% Zn), S-4 (0.35% Zn), and S-5 (0.5% Zn), separately, following the steps above. The metal loading percentage of the catalyst is the proportion of the modified metal element in the dry basis of the feed.

2.2. Characterization of Samples. The crystallographic structures of prepared samples were determined from X-ray diffraction (XRD) patterns collected with a Bruker D8 Advance diffractometer using Cu Kα (k = 1.5406 Å) radiation with a fixed power source (40 kV, 40 mA) and 2θ range from 5° to 50°. The relative crystallinity (%) was calculated from the area in the diffraction angles of 2θ = 23.1°, 23.3°, 23.7°, 23.9°, and 24.4°, where the area of the S-0 sample was defined as 100%. The chemical compositions of the samples were determined by X-ray fluorescence (XRF) spectroscopy on a PANalytical B V Axios-Advanced instrument.

N_2 adsorption−desorption isotherms of the samples were tested using a TPDRO1100 Series apparatus (Thermo Instruments). Before performing the adsorption measurements, the samples were outgassed under a vacuum of 1.33 × 10^{-3} Pa at 300 °C for 12 h. The external surface area and microporous volume were calculated with the BET equation and the t-plot method, respectively. The mesopore size e distributions were calculated with the Barrett−Joyner−Halenda (BJH) equation.

The NH_3-temperature-programmed desorption (TPD) experiments were performed in a Quantachrome automated chemisorption analyzer. The TPD profiles were obtained over a temperature range from 40 to 800 °C at a constant heating rate of 10 °C/min. The pyridine adsorption infrared spectroscopy (Py-IR) of the sample molecular sieve was carried out using an Avatar 360 (Nicolet instrument), which measures the distribution of B acid and L acid on the sample molecular sieve and records the vibration of the molecular sieve skeleton.

The X-ray photoelectron spectroscopy (XPS) of the samples was carried out using an ESCALAB250 (Thermo instrument). The test conditions used were as follows: the Al target was an anode, the test voltage was 10 kV, and the current was 20 mA. The electron binding energy of C 1s of graphite carbon was set to 284.8 eV, and the measured binding energy was corrected by this value.

2.3. Catalyst Testing in the MTA Reaction. The experiment was carried out by using MTA as a model reaction. These prepared molecular sieve catalysts were evaluated in a self-made stainless steel fixed bed reactor (L = 300 mm, Φ16 × 3 mm) under atmospheric pressure at 450 °C, with a single methanol feed. A fixed weight of catalyst (3.5 g) with a 40−60 mesh was put in the constant temperature zone of the stainless steel reactor monitored with a thermocouple and packed with inert filler quartz sand with a 40−60 mesh at both ends. The catalyst was preheated to the desired temperature for 6 h in a flowing nitrogen atmosphere (71 mL/min). The nitrogen gas was turned off at the beginning of the reaction, and the raw material was pumped into the reactor with a liquid weight hourly space velocity (WHSV) of 5 h^{-1}. The reaction was started at 450 °C; the products were condensed and separated by a gas−liquid separator, and the liquid and gas products were analyzed by an EWAI GC-4000A instrument connected to an FID detector and an EWAI GC-4000A instrument equipped with TCD detectors, respectively. The methanol conversion and product selectivity were obtained based on the GC results. The calculation formula is as follows:

$$\text{yield} = \frac{m_{\text{aro}}}{m_{\text{CH}_3\text{OH,in}}} \times 100\%$$

$$\text{selectivity} = \frac{n_i m_i / \text{M}_i}{(m_{\text{CH}_3\text{OH,in}} - m_{\text{CH}_3\text{OH,out}})/M_{\text{CH}_3\text{OH}}} \times 100\%$$

Here, m_{aro} is the mass of aromatics (benzene, methylbenzene, and trimethylbenzene), n_i is the number of C contained in product i, m_i is the mass of product i, and M_i is the relative molecular mass of product i.

3. RESULTS AND DISCUSSION

3.1. Characterization of the ZSM-5 Catalysts. Metal-containing ZSM-5 molecular sieves were prepared by an in situ synthetic method. Figure 1 shows the XRD patterns of different samples each with different diffraction peak intensities but all containing the characteristic peaks of the MFI structure. The introduction of the metal in situ did not change the

https://doi.org/10.1021/acsomega.2c01442
ACS Omega 2022, 7, 24241−24248

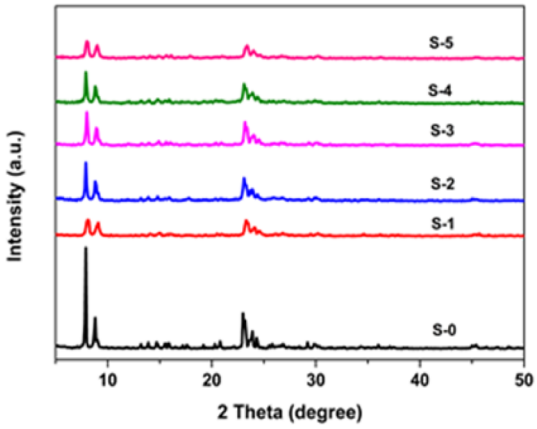

Figure 1. XRD patterns of M/ZSM-5 zeolites by an in situ synthetic method.

structure of the ZSM-5 skeleton. The metal species loading weakened the intensity of the diffraction peak and decreased the crystallinity of the molecular sieve compared with S-0. The different Zn contents led to different amounts of crystallinity in the samples (S-4 > S-3 > S-5), but no significant metal diffraction peaks were observed, indicating that the metal species introduced by the in situ synthetic method were highly dispersed in the molecular sieve or entered the molecular sieve skeleton.[19]

The elemental analysis results in Table 1 showed the silica–alumina ratio of molecular sieve increasing after loading with

Table 1. XRF Analysis of M/ZSM-5 Zeolites by an in Situ Synthetic Method

element/samples	w_{Si} (%)	w_{Al} (%)	w_O (%)	w_M (%)	$n(SiO_2)/n(Al_2O_3)$
S-0	40.33	2.19	57.23		35.34
S-1	40.44	2.17	56.81	0.35	35.80
S-2	41.87	2.25	55.21	0.22	35.79
S-3	42.62	2.27	54.52	0.27	36.09
S-4	41.31	2.16	55.53	0.53	36.78
S-5	41.41	2.19	55.03	0.78	36.31

the metal species compared with the parent ZSM-5, suggesting that the metal species substitution into the molecular sieve framework replaced the aluminum.[2] It was easier for Ga to enter the skeleton than Zn and La, probably because Ga^{3+} and Al^{3+} have similar radii and valence states. The increasing Zn loading ratio increased the Zn content in the bulk phase reaching a maximum when the loading ratio was 0.5%.

The XPS characterization of molecular sieves with different Zn contents is shown in Figure 2. The extracted electron binding energy and the relative content of the elements on the surface of the different Zn-containing molecular sieves are shown in Table 2.

Figure 2 and Table 2 show that the binding energy of the Si 2p and Al 2p peaks increased compared with S-0 for hydrothermally modified molecular sieves, with the shift in the spectrum indicating that the introduction of Zn ions changed the original chemical environment on the surface of the molecular sieve. The peak shape for the Zn element was relatively weak due to the low content of Zn on the surface of the molecular sieve and the influence of the Auger electron peak from the oxygen level near 1017 eV. The electron binding energies of Zn ($2p_{3/2}$) in S-3, S-4, and S-5 were 1022.14, 1022.72, and 1022.45 eV, respectively. The electron binding energy of Zn-halides ($2p_{3/2}$) (electron binding energy = 1022.2–1023.0 eV) is relatively close to and slightly larger than that of the pure ZnO ($2p_{3/2}$) (electron binding energy is 1021.7–1022.5 eV), indicating that the presence of Zn species on the surface of the Zn-loaded molecular sieve might be affected by groups more electronegative than O^{2-}, such as $Zn(OH)^+$, which are favorable for dehydrogenation.[25−27]

Table 2 shows that the growth rate gradually decreased, and the Zn content on the surface of the molecular sieve increased with increasing Zn loading. The chemical content change was related to the amount of Zn in the bulk phase as measured by XRF characterization. The loading ratio of silicon to aluminum on the surface of the molecular sieve gradually decreased with the increase in Zn loading, indicating that the surface of the molecular sieve was desiliconized and supplemented with aluminum, possibly caused by aluminum migration to the surface and enrichment of the molecular sieve framework.

Figure 3 shows the N_2 adsorption–desorption curves for different samples; there are no significant differences between the metal-loaded molecular sieve and the unmodified one. The curves display a type I isotherm, characteristic of the microporous molecular sieve.[6] The tiny hysteresis loops observed with the S-2 molecular sieve might be caused by intergranular intervals. Table 3 shows the specific surface area and micropore volume of the molecular sieves reduced after metal loading, which could be metal species occupying the surface and channels, subtly altering the texture properties of the zeolite.

The concentration and strength of acid sites in different samples were determined by NH_3-TPD; the results are shown in Figure 4. Generally, an NH_3-TPD profile from a zeolite exhibits two desorption peaks, at high (above 450 °C) and low (below 400 °C) temperatures, ascribed to ammonia adsorbed on the strong and weak acid sites, respectively. In this work, the distribution of the acid sites across the two acidic strengths was determined by integrating the NH_3-TPD profiles in different temperature intervals. These profiles are listed in Table 4, where the quantities of strong and weak acid sites were measured by the amounts of ammonia desorbed over 450–600 and 200–350 °C.

After the introduction of metal by the hydrothermal method, the loading of Ga causes a larger shift in the acid center position than that of La or Zn; as the Zn loading increases, the proportion of the weak acid peak area increases, and the ratio of strong acid peak area decreases, possibly due to the Zn species existing on the surface of the molecular sieve in the form of $ZnOH^+$ (or other forms observed by XPS) that covers a part of the strong acid center or turns the strong acid center into a weak acid center.

The FT-IR spectrum in Figures 5a and 6a showed that the prepared molecular sieves all have the characteristic ZSM-5 structure, and the peak positions of other samples were shifted compared with S-0 due to the metals entering the molecular sieve framework; however, the relatively low metal loading causes the peak shift to be minimal.

As seen in Figure 5b, the strong absorption bands of S-0 appeared at the five peak positions 1450, 1490, 1540, 1625, and 1635 cm^{-1}.[28] The peaks at 1450 and 1625 cm^{-1} are caused by the L acid on the molecular sieve, and the peak at 1540 cm^{-1} can be attributed to the B acid on the molecular sieve; the peaks at 1490 and 1635 cm^{-1} are the results of the

https://doi.org/10.1021/acsomega.2c01442
ACS Omega 2022, 7, 24241−24248

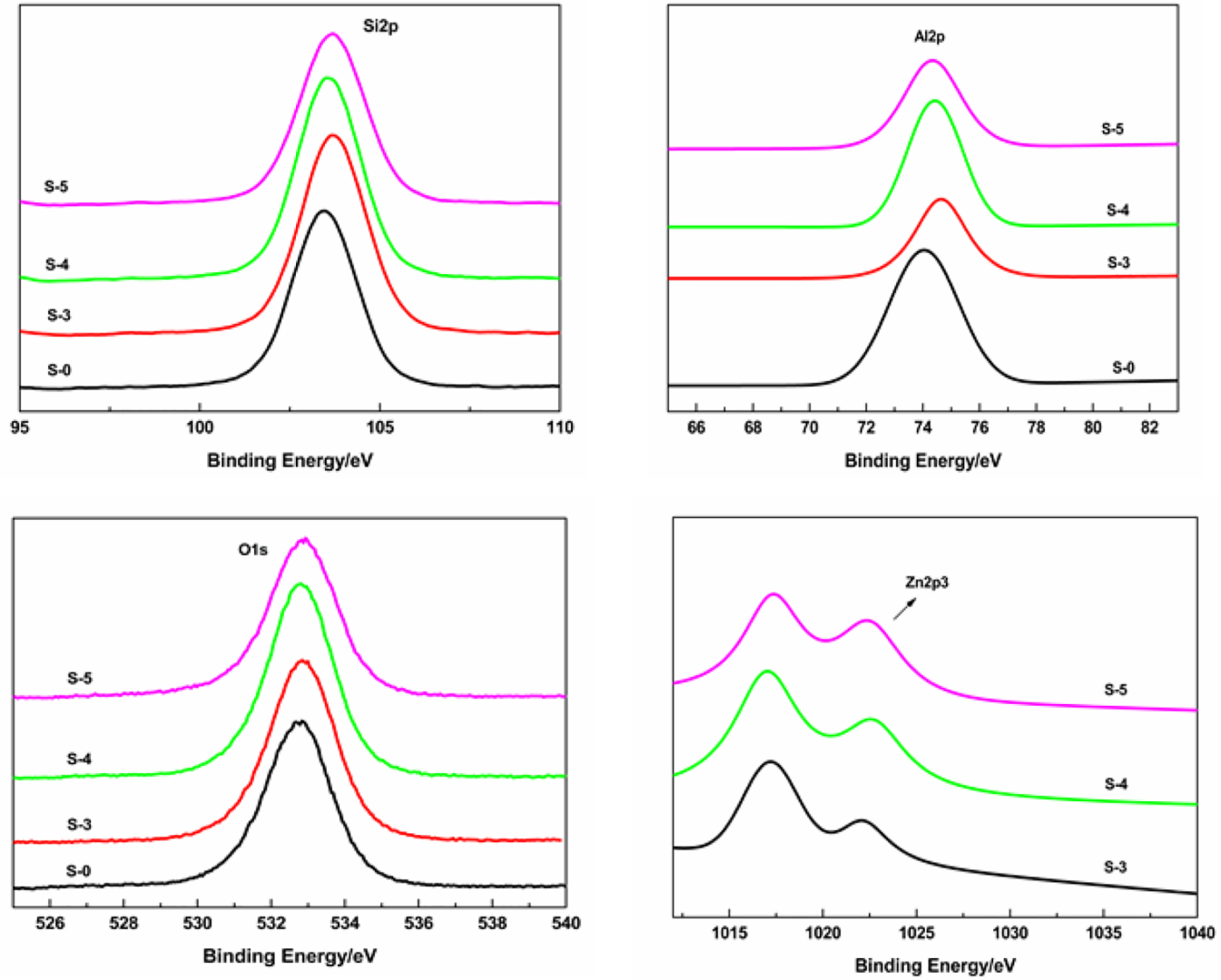

Figure 2. XPS spectra of HZSM-5 zeolites under different Zn contents.

Table 2. XPS Analysis of Surface Elements of HZSM-5 Zeolites under Different Zn Contents

	electron binding energy/eV				surface relative content/%				
sample	Si 2p	Al 2p	O 1s	Zn $2p_3$	w_{Si} (%)	w_{Al} (%)	w_O (%)	w_{Zn} (%)	$n(SiO_2)/n(Al_2O_3)$
S-0	103.35	74.04	532.75		24.86	2.31	72.84		20.67
S-3	103.65	74.65	532.85	1022.14	26.35	1.87	71.58	0.20	26.98
S-4	103.55	74.45	532.80	1022.72	24.16	2.25	73.30	0.29	20.60
S-5	103.45	74.25	532.86	1022.45	24.95	2.42	72.30	0.34	19.79

interaction of the B acid and L acid.[29] After adding Zn, the absorption peak at 1625 cm^{-1} shifted to 1616 cm^{-1}, but this shift was not observed with the addition of Ga or La. Other studies have seen the peak at 1616 cm^{-1} with the introduction of Zn species. Figure 5c shows two obvious hydroxyl vibration bands on S-0: one is the vibrational peak of aluminum hydroxy at 3610 cm^{-1}, with strong B acidity, and the other was the terminal silicon oxyhydroxide at 3740 cm^{-1}.[30,31] The vibration peak did not change with the ion exchange and can be used as a reference. After hydrothermal modification, the vibration of the molecular sieve at 3610 cm^{-1} weakened, indicating that the hydrothermal modification would lead to the reduction of the B acid.

Figure 6 shows a pyridine adsorption infrared spectrum and a hydroxyl group spectrum from a sample molecular sieve catalyst. The effect of Zn content on the intensity of each peak in Figure 6b shows that the peak intensities of 1450 and 1616 cm^{-1} are positively correlated with the Zn content, and the peak intensities of 1490, 1540, and 1635 cm^{-1} are negatively correlated with the Zn content. These results are a further indication that the peaks at 1450 and 1616 cm^{-1} were caused by the L acid, that the Zn increase enhanced the L acid peak, and that the B acid peak was weakened. Figure 6c shows two hydroxyl vibration bands at 3610 and 3740 cm^{-1} on the samples.[32] The introduction of Zn did not create a new measurable hydroxyl vibration peak, indicating that Zn does not form hydroxy Zn ions ($Zn(OH)^+$) on aluminum hydroxyl

https://doi.org/10.1021/acsomega.2c01442
ACS Omega 2022, 7, 24241−24248

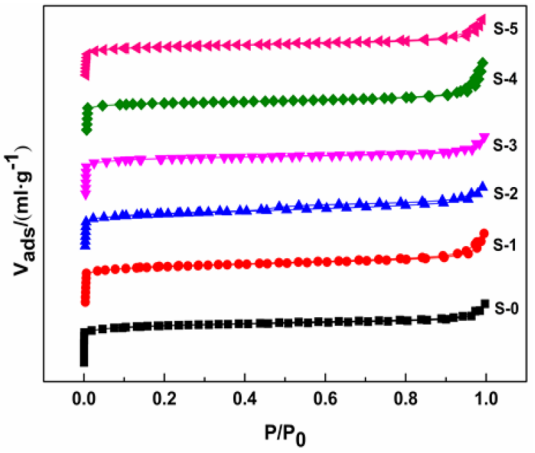

Figure 3. N_2 adsorption−desorption isotherms of different samples.

Table 3. Texture Properties of Different Samples

samples	S_{BET} (m^2/g)	S_{micro} (m^2/g)	V_{total} (mL/g)	$D_{average}$ (nm)	V_{micro} (mL/g)	D_{HK} (nm)
S-0	399	356	0.260	2.61	0.161	0.98
S-1	378	312	0.302	3.20	0.158	1.25
S-2	345	267	0.260	3.02	0.146	1.24
S-3	397	337	0.258	2.59	0.149	1.28
S-4	295	235	0.297	4.04	0.119	1.45
S-5	307	258	0.244	3.17	0.114	1.34

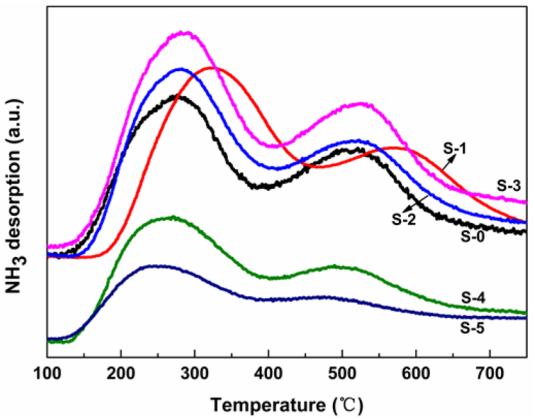

Figure 4. NH_3-TPD patterns of different samples.

groups. The increase in Zn content does cause a weakening in the vibrational peak of the aluminum hydroxy group, indicating that Zn does interact with the aluminum hydroxy group on the molecular sieve.

Table 5 shows that the amount of B acid decreased slightly when Zn is added, but the amount of L acid increased significantly, possibly due to the formation of new Zn-L acid by Zn^{2+} and molecular sieves,[25] and the number of L acid sites increased by adding Ga. While adding La, the L acid showed minimal change, possibly because Zn and Ga filled the outermost d electron orbital. The introduction of Zn^{2+} and Ga^{3+} makes the original electrons in the molecular sieve framework tend toward metal ions attracted by the electrostatic field of the extranuclear electrons of the metal cation, which will activate the hydroxyl groups on the molecular sieve framework to a certain extent and change the acid properties, especially for L acid. When adding La, the amount of B acid on the surface of the molecular sieve was obviously reduced. Maybe the introduction of the metal was predominately in the form of an oxide that covered a part of the proton active sites on the molecular sieve. As the Zn loading increases, the B acid decreases, and the L acid increases.

3.2. Catalytic Performance of the Catalysts. The aromatization performance of the above-mentioned catalysts was evaluated under normal pressure using a single methanol feed, a reaction temperature of 450 °C, and a WHSV of 5 h^{-1}. Figure 7 shows that the methanol conversion of S-1, S-2, and S-3 reached approximately 100% within the 5 h reaction time with different aromatics yields S-3 > S-1 > S-2. The lower content of Zn significantly enhanced the aromatics yield, a 4% increase compared with S-0, and the highest yields of S-2 and S-1 did not increase much, possibly because the Zn modification reduced the amount of B acid and significantly increased the amount of L acid, while both the B and L acids of modified Ga and La zeolites were simultaneously reduced. Compared with the Ga and La, the Zn sites and the acid sites in ZSM-5 zeolite have a stronger interaction and accessibility, which can effectively promote the formation of L acid sites. The regulation of the surface acidity by the metal on the molecular sieve was directly related to the hydrogen transfer and the dehydrogenation process. The improvement in dehydrogenation aromatization performance of the L acid after Zn modification compensated for the weakening of the hydrogen transfer aromatization of the B acid, resulting in a significant increase in the yield. The modification using Ga and La was simultaneously weakened, and there was little change in the yield of aromatic hydrocarbons with no side effects. Therefore, Zn is a more suitable metal species for hydrothermal modification under the synthetic conditions of this experiment.

As the Zn loading increased, the yield of aromatics initially increased and then decreased with the loading of S-4 being optimal. A suitable Zn loading improved the stability of the catalyst; however, too much or too little loading decreased the working life of the catalyst due to the pore structure of the molecular sieve. The pore size and pore volume were the largest when the loading was 0.35%, where the larger pore size and developed channels reduce the effect of coking, prolong

Table 4. Comparison of Strong/Weak Acid of Different Samples

sample	total acid amount/mmol g^{-1}	weak acid peak/ °C	strong acid peak/ °C	weak acid peak area fraction/%	strong acid peak area fraction/%	strong acid/weak acid
S-0	1.23	270	500	58.15	41.85	0.720
S-1	1.23	323	567	63.16	36.84	0.583
S-2	1.09	279	508	59.21	40.79	0.689
S-3	1.33	282	511	62.65	37.35	0.596
S-4	0.89	265	492	63.32	36.68	0.579
S-5	0.73	249	469	66.38	33.62	0.507

https://doi.org/10.1021/acsomega.2c01442
ACS Omega 2022, 7, 24241−24248

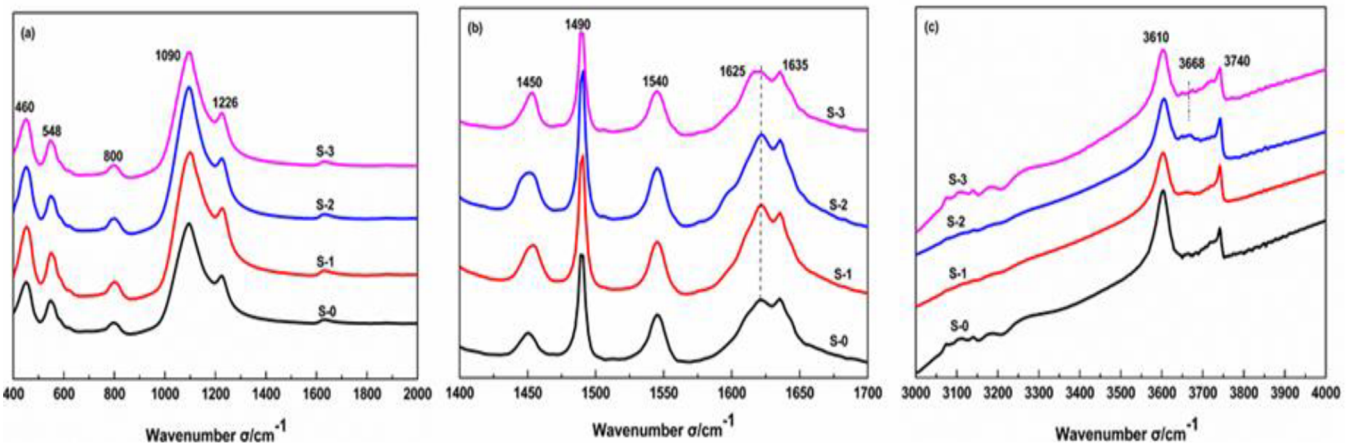

Figure 5. IR spectra of different samples: (a) skeleton IR spectra, (b) Py-IR spectra, and (c) IR spectra of hydroxyl.

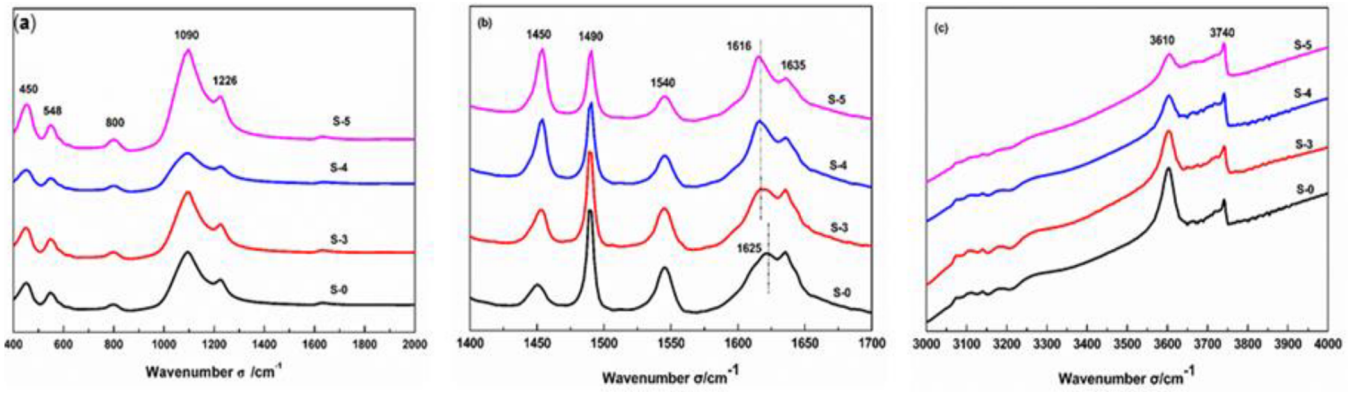

Figure 6. IR spectra of different samples with different Zn loading: (a) skeleton IR spectra, (b) Py-IR spectra, and (c) IR spectra of hydroxyl.

Table 5. Acid Distribution of Different Samples

sample	B acid	L acid	B/L
S-0	0.265	0.127	2.294
S-1	0.160	0.115	1.393
S-2	0.179	0.120	1.486
S-3	0.233	0.190	1.466
S-4	0.174	0.330	0.695
S-5	0.137	0.378	0.509

the life of the molecular sieve, and improve the stability. Figure 8a demonstrates the effect of the B/L value on the molecular sieve selectivity of aromatics after a 2 h time on stream. The B/L value decreased as the Zn content increased, and the aromatic hydrocarbon selectivity first increased and then decreased. Figure 8b shows that, with increased Zn loadings, the low carbon olefin selectivity increased. The authors suggest that the introduction of Zn covers the original B acid, resulting in a decrease of the center of the B acid that inhibits the gathered olefin and suppresses the aromatics alkylation reaction. The increased selectivity for high carbon aromatics is more likely to lead to catalyst coking and a reduction in the stability of the catalyst.

As shown in Figure 9, the generation of aromatics can be divided into two pathways: (a) cycloalkane and alkene hydrogen transfer (HT) at the B acid site and (b) cycloalkane dehydrogenation (DH) at the Zn-L acid site. When the loading is less than 0.15%, the acid content of B is higher than that of L acid, and a is more dominant than b; the selectivity of alkanes in the product is high, and the selectivity of BTX is low. When the loading is between 0.15 and 0.35, the B/L is reduced to about 0.7, and the aromatics selectivity is obviously improved under the cooperation of the two. When the load increases to 0.5, the advantage of route b is obvious, and the olefin selectivity increases significantly; however, the increase in CO + CO_2 selectivity indicates that the proportion of methanol decomposition increases, accelerating catalyst deactivation, and the aromatics selectivity drops instead. It can be seen that B/L needs to be within a certain appropriate range, and the two pathways can match each other to play the best role. Therefore, in this work, when the value of B/L was 0.695, the reaction of methanol to aromatic hydrocarbons was most favorable, giving the highest selectivity to aromatics and providing excellent stability.

4. CONCLUSION

ZSM-5 molecular sieves containing Zn, La, and Ga and with different Zn contents were synthesized by the in situ synthetic method, and their textural and acidic properties and catalytic performance in MTA were investigated. The results indicated that the acid distribution was associated with the aromatics yield and was significantly influenced by the type and amount of metal. Zn was the most favorable metal for the MTA reaction. When the loading is 0.35%, the aromatics selectivity reaches 56%, 26% higher than the parent ZSM-5. The in situ synthesis method used in this work provides a more convenient and efficient method for synthesizing metal–

https://doi.org/10.1021/acsomega.2c01442
ACS Omega 2022, 7, 24241−24248

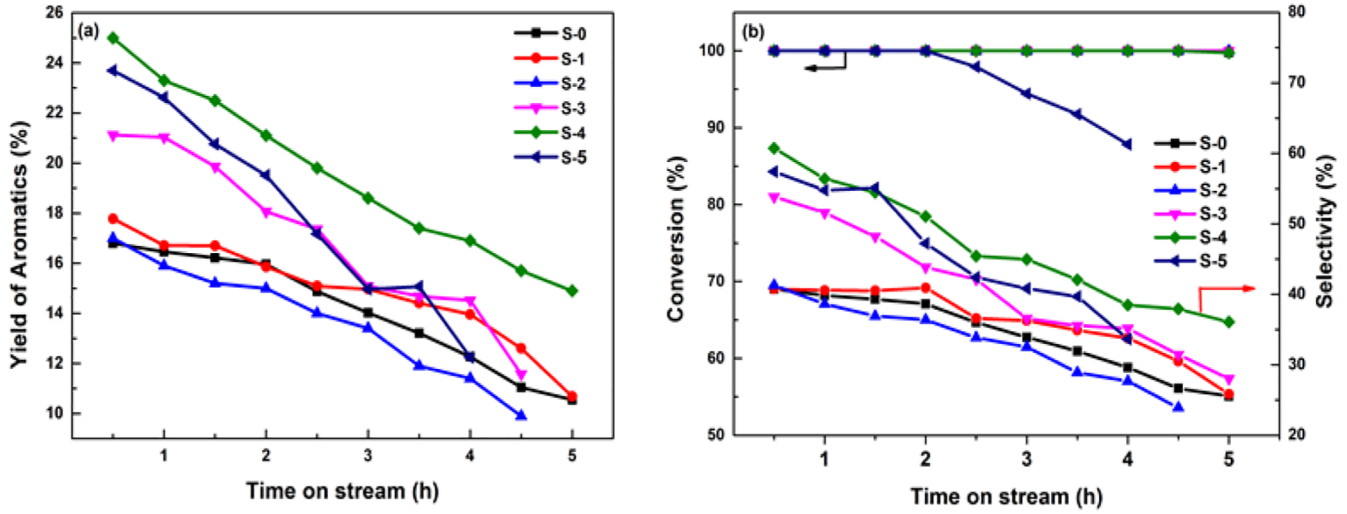

Figure 7. (a) Aromatization properties of different samples. (b) Aromatization properties of different samples.

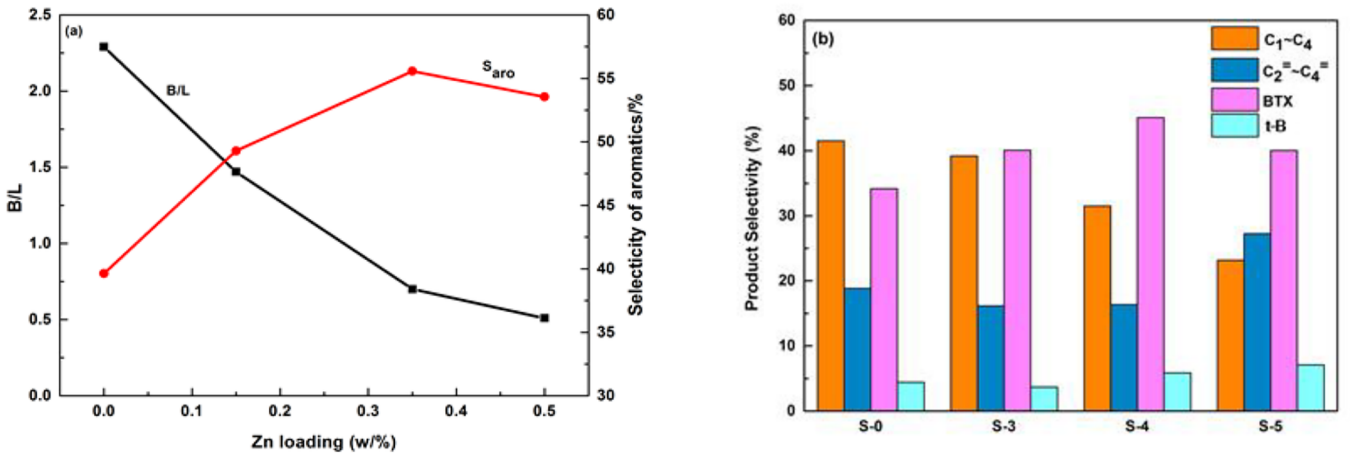

Figure 8. (a) Effect of B/L ratio on the selectivity of aromatics. (b) Product selectivity of different samples.

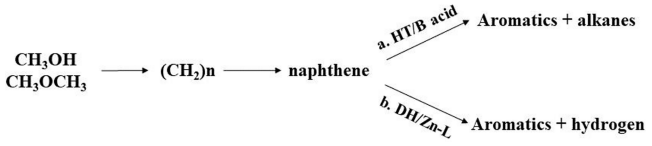

Figure 9. Brief reaction pathway to generate aromatics in the MTA reaction on Zn/ZSM-5.

zeolite bifunctional catalysts, which is more conducive to the industrial production of catalysts.

AUTHOR INFORMATION

Corresponding Author

Jianwei Li − *State Key Laboratory of Chemical Resources Engineering, Beijing University of Chemical Technology, Beijing 100029, China;* orcid.org/0000-0002-1722-1251; Email: lijw@mail.buct.edu.cn

Authors

Yanjun Zhang − *State Key Laboratory of Chemical Resources Engineering, Beijing University of Chemical Technology, Beijing 100029, China*

Yao Liu − *State Key Laboratory of Chemical Resources Engineering, Beijing University of Chemical Technology, Beijing 100029, China*

Complete contact information is available at: https://pubs.acs.org/10.1021/acsomega.2c01442

Notes

The authors declare no competing financial interest.

ACKNOWLEDGMENTS

This work was financially supported by the National Key R&D Program of China (2018YFB0604802).

REFERENCES

(1) Yarulina, I.; Chowdhury, A. D.; Meirer, F.; Weckhuysen, B. M.; Gascon, J. Recent trends and fundamental insights in the methanol-to-hydrocarbons process. *Nat. Catal* **2018**, *1* (6), 398−411.

(2) Pinilla-Herrero, I.; Borfecchia, E.; Holzinger, J.; Mentzel, U. V.; Joensen, F.; Lomachenko, K. A.; Bordiga, S.; Lamberti, C.; Berlier, G.; Olsbye, U.; Svelle, S.; Skibsted, J.; Beato, P. High Zn/Al ratios enhance dehydrogenation vs hydrogen transfer reactions of Zn-ZSM-5 catalytic systems in methanol conversion to aromatics. *J. Catal.* **2018**, *362*, 146−163.

https://doi.org/10.1021/acsomega.2c01442
ACS Omega 2022, 7, 24241−24248

(3) Zhang, G. Q.; Bai, T.; Chen, T. F.; Fan, W. T.; Zhang, X. Conversion of Methanol to Light Aromatics on Zn-Modified Nano-HZSM-5 Zeolite Catalysts. *Ind. Eng. Chem. Res.* **2014**, *53* (39), 14932−14940.
(4) Ilias, S.; Bhan, A. Mechanism of the Catalytic Conversion of Methanol to Hydrocarbons. *ACS Catal.* **2013**, *3* (1), 18−31.
(5) Bi, Y.; Wang, Y.; Chen, X.; Yu, Z.; Xu, L. Methanol aromatization over HZSM-5 catalysts modified with different zinc salts. *Chin J. Catal* **2014**, *35* (10), 1740−1751.
(6) Yang, L.; Liu, Z.; Liu, Z.; Peng, W.; Liu, Y.; Liu, C. Correlation between H-ZSM-5 crystal size and catalytic performance in the methanol-to-aromatics reaction. *Chin J. Catal* **2017**, *38* (4), 683−690.
(7) Gong, Q.; Fang, T.; Xie, Y.; Zhang, R.; Liu, M.; Barzagli, F.; Li, J.; Hu, Z.; Zhu, Z. High-Efficiency Conversion of Methanol to BTX Aromatics Over a Zn-Modified Nanosheet-HZSM-5 Zeolite. *Ind. Eng. Chem. Res.* **2021**, *60* (4), 1633−1641.
(8) Gao, P.; Xu, J.; Qi, G.; Wang, C.; Wang, Q.; Zhao, Y.; Zhang, Y.; Feng, N.; Zhao, X.; Li, J.; Deng, F. A Mechanistic Study of Methanol-to-Aromatics Reaction over Ga-Modified ZSM-5 Zeolites: Understanding the Dehydrogenation Process. *ACS Catal.* **2018**, *8* (10), 9809−9820.
(9) Jia, Y.; Wang, J.; Zhang, K.; Liu, S.; Chen, G.; Yang, Y.; Ding, C.; Liu, P. Catalytic conversion of methanol to aromatics over nano-sized HZSM-5 zeolite modified by ZnSiF6 center dot 6H(2)O. *Catal. Sci. Technol.* **2017**, *7* (8), 1776−1791.
(10) Olsbye, U.; Svelle, S.; Bjørgen, M.; Beato, P.; Janssens, T. V. W.; Joensen, F.; Bordiga, S.; Lillerud, K. P. Conversion of Methanol to Hydrocarbons: How Zeolite Cavity and Pore Size Controls Product Selectivity. *Angew. Chem. Int. Ed* **2012**, *51* (24), 5810−5831.
(11) Olson, D. H.; Kokotailo, G. T.; Lawton, S. L.; Meier, W. M. Crystal structure and structure-related properties of ZSM-5. *J. Phys. Chem. B* **1981**, *85*, 2238.
(12) Xing, A. H.; Sun, Q. Advances in catalysts for methanol to aromatics. *Modern Chemical Industry* **2013**, *33* (3), 29−34.
(13) Li, J.; Liu, S.; Zhang, H.; Lü, E.; Ren, P.; Ren, J. Synthesis and characterization of an unusual snowflake-shaped ZSM-5 zeolite with high catalytic performance in the methanol to olefin reaction. *Chin J. Catal* **2016**, *37* (2), 308−315.
(14) Kokotailo, G. T.; Lawton, S. L.; Olson, D. H. Structure of synthetic zeolite ZSM-5. *Nature* **1978**, *272* (5652), 437−438.
(15) Conte, M.; Lopezsanchez, J. A.; He, Q.; Morgan, D. J.; Ryabenkova, Y.; Bartley, J. K.; Carley, A. F.; Taylor, S. H.; Kiely, C. J.; Khalid, K. Modified zeolite ZSM-5 for the methanol to aromatics reaction. *Catal. Sci. Technol.* **2012**, *2* (1), 105−112.
(16) Sun, A. M.; You-Ming, N. I.; Li-Juan, O. U.; Guang-Xing, L. I. Study on ethanol aromatization performance of alkali treated and Zn modified ZSM-5 zeolites. *Appl. Chem. Ind.* **2015**, *1*, 95−98.
(17) Ogura, M.; Shinomiya, S.-y.; Tateno, J.; Nara, Y.; Nomura, M.; Kikuchi, E.; Matsukata, M. Alkali-treatment technique - new method for modification of structural and acid-catalytic properties of ZSM-5 zeolites. *Appl. Catal, A General* **2001**, *219* (1), 33−43.
(18) Bjørgen, M.; Joensen, F.; Holm, M. S.; Olsbye, U.; Lillerud, K. P.; Svelle, S. Methanol to gasoline over zeolite H-ZSM-5: Improved catalyst performance by treatment with NaOH. *Appl. Catal., A* **2008**, *345* (1), 43−50.
(19) Pan, D.; Song, X.; Yang, X.; Gao, L.; Xiao, G. Efficient and selective conversion of methanol to para-xylene over stable H[Zn,Al]-ZSM-5/SiO2 composite catalyst. *Appl. Catal., A* **2018**, *557*, 15−24.
(20) Niu, X.; Gao, J.; Miao, Q.; Dong, M.; Wang, G.; Fan, W.; Qin, Z.; Wang, J. Influence of preparation method on the performance of Zn-containing HZSM-5 catalysts in methanol-to-aromatics. *Microporous Mesoporous Mater.* **2014**, *197*, 252−261.
(21) Su, X.; Zhang, K.; Snatenkova, Y.; Matieva, Z.; Wu, W. High-efficiency nano [Zn,Al]ZSM-5 bifunctional catalysts for dimethyl ether conversion to isoparaffin-rich gasoline. *Fuel Process. Technol.* **2020**, *198*, 106242.
(22) Niu, X.; Gao, J.; Miao, Q.; Dong, M.; Wang, G.; Fan, W.; Qin, Z.; Wang, J. Influence of preparation method on the performance of Zn-containing HZSM-5 catalysts in methanol-to-aromatics. *Microporous Mesoporous Mater.* **2014**, *197*, 252−261.
(23) Su, X.; Wang, G.; Ba, X., I; Wei, W.; Xiao, L.; Fang, Y.; Zhang, J. Synthesis of nanosized HZSM-5 zeolites isomorphously substituted by gallium and their catalytic performance in the aromatization - ScienceDirect. *Chem. Eng. J.* **2016**, *293*, 365−375.
(24) Zhang, S.; Yang, M.; Shao, J.; Yang, H.; Zeng, K.; Chen, Y.; Luo, J.; Agblevor, F.; Chen, H. The conversion of biomass to light olefins on Fe-modified ZSM-5 catalyst: Effect of pyrolysis parameters. *Sci. Total Environ.* **2018**, *628*, 350−357.
(25) Niu, X.; Gao, J.; Wang, K.; Miao, Q.; Dong, M.; Wang, G.; Fan, W.; Qin, Z.; Wang, J. Influence of crystal size on the catalytic performance of H-ZSM-5 and Zn/H-ZSM-5 in the conversion of methanol to aromatics. *Fuel Proces. Technol.* **2017**, *157*, 99−107.
(26) Chen, J.; Chang, L.; Rang, H.; Ding, F. X. Characterization of Zn promoter in ZnO/HZSM-5 catalyst for propane aromatization. *Chin J. Catal* **2001**, *22* (3), 229−232.
(27) Gao, J.; Wei, C.; Dong, M.; Wang, G.; Li, Z.; Qin, Z.; Wang, J.; Fan, W. Evolution of Zn Species on Zn/HZSM-5 Catalyst under H2 Pretreated and its Effect on Ethylene Aromatization. *ChemCatChem.* **2019**, *11* (16), 3892−3902.
(28) Kim, Y. H.; Lee, K. H.; Lee, J. S. The effect of pre-coking and regeneration on the activity and stability of Zn/ZSM-5 in aromatization of 2-methyl-2-butene. *Catal. Today* **2011**, *178* (1), 72−78.
(29) Parry, E. P. An infrared study of pyridine adsorbed on acidic solids. Characterization of surface acidity. *J. Catal.* **1963**, *2* (5), 371−379.
(30) Karge, H. G.; Dondur, V. Investigation of the distribution of acidity strength in zeolites by temperature-programmed desorption of probe molecules. 2. Dealuminated Y-type zeolites. *J. Phys. Chem.* **1991**, *94* (2), 12.
(31) Zhang, Y.; Qu, Y.; Wang, D.; Zeng, X. C.; Wang, J. Cadmium Modified HZSM-5: A Highly Efficient Catalyst for Selective Transformation of Methanol to Aromatics. *Ind. Eng. Chem. Res.* **2017**, *56* (44), 12508−12519.
(32) Tian, H.; Jiao, J.; Tian, H.; He, H.; Zha, F.; Guo, X.; Tang, X.; Chang, Y. Methanol aromatization over Zn-modified HZSM-5 catalysts derived from ZIF-8. *Fuel* **2021**, *302*, 121224.

https://doi.org/10.1021/acsomega.2c01442
ACS Omega 2022, 7, 24241−24248